

Article

The Synergistic Effect of Pyridinic Nitrogen and Graphitic Nitrogen of Nitrogen-Doped Graphene Quantum Dots for Enhanced TiO₂ Nanocomposites' Photocatalytic Performance

Fei Li ¹, Ming Li ², Yi Luo ¹, Ming Li ^{1,*}, Xinyu Li ¹, Jiye Zhang ³ and Liang Wang ^{2,*} 

¹ College of Science, Guilin University of Technology, Guilin 541004, China; m17753101516@163.com (F.L.); adam2513@163.com (Y.L.); lixinyu5260@163.com (X.L.)

² Institute of Nanochemistry and Nanobiology, School of Environmental and Chemical Engineering, Shanghai University, Shanghai 200444, China; limingdobest@163.com

³ School of Materials Science and Engineering, Shanghai University, Shanghai 200444, China; jychang@shu.edu.cn

* Correspondence: liming928@163.com (M.L.); wangl@shu.edu.cn (L.W.);
Tel.: +86-773-369-6613 (M.L.); +86-021-661-3526 (L.W.)

Received: 9 September 2018; Accepted: 30 September 2018; Published: 4 October 2018



Abstract: In this study, nitrogen-doped graphene quantum dots (N-GQDs) and a TiO₂ nanocomposite were synthesized using a simple hydrothermal route. Ammonia water was used as a nitrogen source to prepare the N-GQDs. When optically characterized by UV-vis, N-GQDs reveal stronger absorption peaks in the range of ultraviolet (UV) light than graphene quantum dots (GQDs). In comparison with GQDs/TiO₂ and pure TiO₂, the N-GQDs/TiO₂ have significantly improved photocatalytic performance. In particular, it was found that, when the added amount of ammonia water was 50 mL, the content of pyridinic N and graphitic N were as high as 22.47% and 31.44%, respectively. Most important, the photocatalytic activity of N-GQDs/TiO₂-50 was about 95% after 12 min. The results illustrated that pyridinic N and graphitic N play a significant role in photocatalytic performance.

Keywords: N-doped graphene quantum dots; TiO₂; photocatalytic performance; pyridinic N; graphitic N

1. Introduction

In recent decades, increasing environmental pollution has attracted more and more attention, especially the discharge of dye wastewater from factories. It is therefore appropriate to find an effective, low-cost and pollution-free replacement for traditionally problematic energy production. Photocatalysis could be one of the most effective measures to solve the problems of energy shortage and environmental pollution [1–4]. In many semiconductor metal oxide materials, for example, titanium dioxide (TiO₂) is extensively used as a photocatalyst [5–7], due to its beneficial characteristics. It is inexpensive, non-poisonous, and has excellent chemical and physical stability [5,8]. Although it has so many superior properties, use of TiO₂ as a photocatalyst is limited by some disadvantages in practical application, such as a wide band gap (3.2 eV) and a high electron-hole recombination rate, which leads to low photocatalytic efficiency [3,9–11]. To perfect the photocatalytic activity of TiO₂, various measures were utilized, such as many ions being doped into the lattice of TiO₂ [12], sensitization via absorbed molecules [13–15], compound with other materials [16,17], and the surface being coated with other cocatalysts possessing excellent performance [18–21]. Among the methods mentioned above, surface loading with other cocatalysts is relatively facile and effective in enhancing the photocatalytic

activity of TiO₂. Although some auxiliary catalysts can improve the photocatalytic performance of TiO₂, for instance Pt, Au and Ag, their high cost limits their application [22,23]. Therefore, it would be significant to find highly efficient, simple and eco-friendly cocatalysts which enhance the photocatalytic performance of TiO₂.

Graphene quantum dots (GQDs) are a novel kind of 0D carbon nanomaterial with dimensions below 10 nm. In addition to all the properties of graphene, GQDs also have unique edge effects and quantum confinement [24]. GQDs are widely used in various fields due to their excellent physical and chemical properties. They are used in photovoltaic devices [25], catalysis [26–30], drug delivery [31], and cell imaging [32–35]. GQDs are environmentally friendly materials with strong anti-chemical corrosion and anti-ultraviolet (UV) irradiation capabilities. Pure GQDs display low catalytic activity due to their high exciton binding energy [36]. In many past studies, GQDs as auxiliary catalysts effectively improved the photocatalytic performance of TiO₂ [37], and some reports showed that the doped GQDs displayed excellent effects on improving the photocatalytic performance of TiO₂, for example, when nitrogen [38], sulfur [3] and nitrogen and sulfur co-doped [39]. However, there is little work on the effect of different N-bonding structure for the photocatalytic performance of nitrogen-doped GQDs (N-GQDs).

In our study, N-GQDs with different N contents were synthesized by a facile hydrothermal stratagem using different volumes of ammonia water and GQDs. N-GQDs were attached tightly to the surface of TiO₂ with a facile hydrothermal method. The photocatalytic performance of N-GQDs/TiO₂ was tested by introducing methyl orange (MO). A possible mechanism for improving photocatalytic performance was also investigated and analyzed by comparing the photocatalytic effect of N-GQDs/TiO₂ and pure TiO₂. All the results showed that N-GQDs effectively improved the photocatalytic performance of TiO₂, in which pyridinic N and graphitic N play a decisive role. This work may provide a new perspective for the future study of complexes based on N-GQDs.

2. Results and Discussion

Unless otherwise specified, the N-GQDs-50 with the best optical performance was selected for various characterizations.

2.1. Morphology and Structural Characterization of GQDs and N-GQDs

Figure 1a–d displays the transmission electron microscopy (TEM) and high resolution transmission electron microscopy (HRTEM) images of GQDs and N-GQDs-50. Figure 1a,b shows the TEM images of GQDs and N-GQDs-50, and the size distribution is homogeneous. The size of GQDs and N-GQDs-50 ranged from 2–16 nm and 1–5 nm, the average diameter was 8.66 nm and 3.12 nm respectively (insert in Figure 1a,b). The reduction in the size of N-GQDs-50 was likely to be due to further decomposition of GQDs during the subsequent hydrothermal reaction (refer to the experiment for details). The HRTEM images show that the plane lattice spacing of GQDs and N-GQDs-50 was 0.21 nm, which is similar to the in-plane lattice spacing of graphite (002) [40,41]. Figure 1e shows a TEM image of TiO₂ nanoparticles with the thin film. After the hydrothermal reaction, the N-GQDs were compounded on the surface of TiO₂. With the oxygen-containing functional groups of N-GQDs, the hydroxyl functional groups of TiO₂ may be able to construct functional and relatively stable composites.

XRD was employed to determine the crystalline structure of GQDs and N-GQDs-50. It was clear from the pattern (Figure 2a) of pure TiO₂ that there were two types of TiO₂, namely anatase and rutile. Peaks at $2\theta = 25.6^\circ, 37.18^\circ, 48.25^\circ, 54.02^\circ, 55.24^\circ$ and 62.7° represented (101), (004), (200), (105), (211) and (116) planes of anatase. Others at 41.44° and 56.82° , represented (110) and (114) of rutile, which identified with P25. The XRD pattern of N-GQDs-50 showed the peaks of N-GQDs/TiO₂-50 were the same as that of TiO₂, indicating that the structure of TiO₂ was not affected by N-GQDs. FT-IR spectroscopy can also characterize samples. As shown in Figure 2b, broad absorption bands at 480–700 cm⁻¹ were associated with stretching vibrations of Ti-O-Ti and Ti-O-C. The peak at 1380 cm⁻¹ was related to nitrate ion and

the peak at 1633 cm^{-1} was due to $\delta\text{H}_2\text{O}$ vibration of the water molecule [42]. The figures of FT-IR indicated that N-GQDs was successfully coupled with TiO_2 .

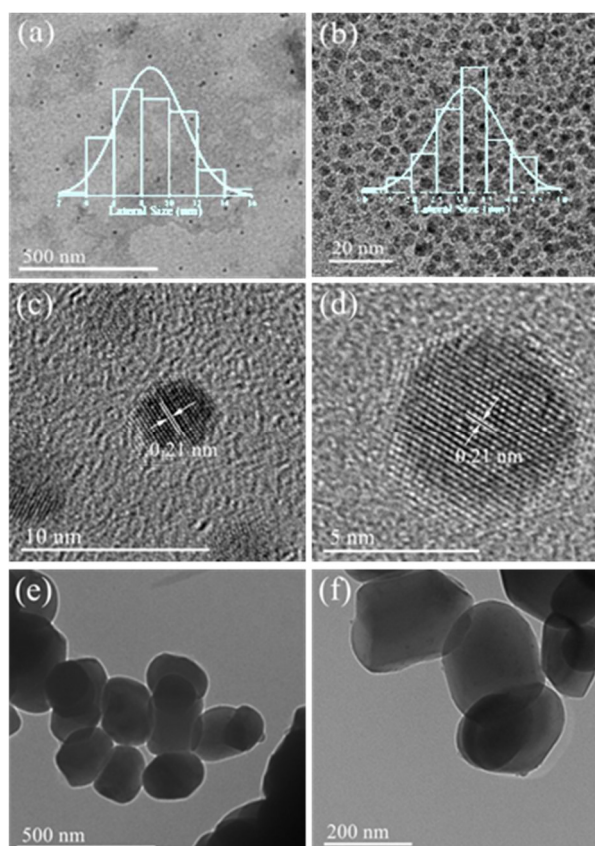


Figure 1. TEM images of GQDs (a), N-GQDs-50 (b), TiO_2 (e) and N-GQDs/ TiO_2 -50 (f), insets are of corresponding lateral size distribution. HRTEM images of GQDs (c) and N-GQDs-50 (d).

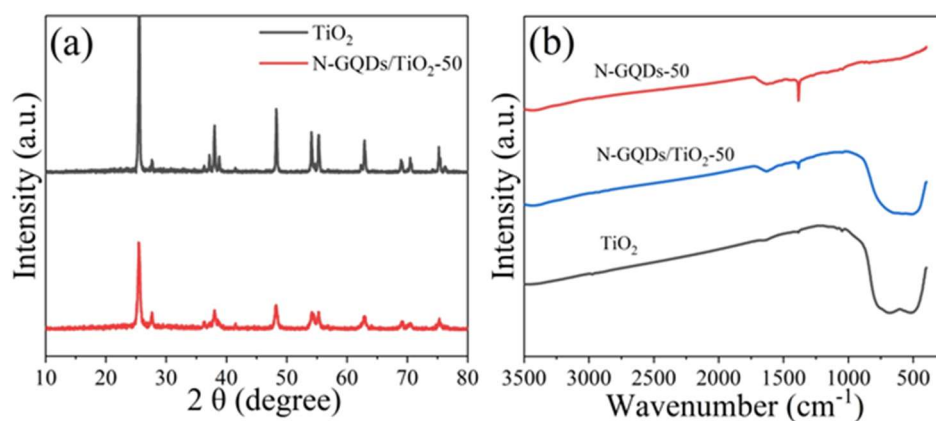


Figure 2. XRD pattern (a) of pure TiO_2 and N-GQDs/ TiO_2 -50; FT-IR spectra (b) of pure TiO_2 , N-GQDs-50 and N-GQDs/ TiO_2 -50 composites.

To further investigate the composition of GQDs and N-GQDs, XPS (X-ray photoelectron spectroscopy) measurement was employed. Figure 3a shows the full XPS spectra of GQDs, N-GQDs-50 and N-GQDs-100. Peaks can be seen at approximately 284 eV (C 1s), 399.08 eV (N 1s) and 531.08 eV (O 1s) in all the samples. Compared to GQDs, the intensity of N 1s peak N-GQDs-50 and N-GQDs-100 was relatively enhanced, indicating that the N was successfully doped into the GQDs through the hydrothermal reaction with ammonia water. The results in Table 1 further show that the N content of N-GQDs-50 and N-GQDs-100 was higher than GQDs, and the content of N-GQDs-50 was the highest,

reaching 10.64%, also indicating that N-GQDs were synthesized successfully. The high-resolution spectrum of N 1s region of N-GQDs-50 and N-GQDs-100 was divided into three peaks at 398.9 eV (pyridinic N), 399.6 eV (pyrrolic N) and 401.5 eV (graphitic N) [25,43].

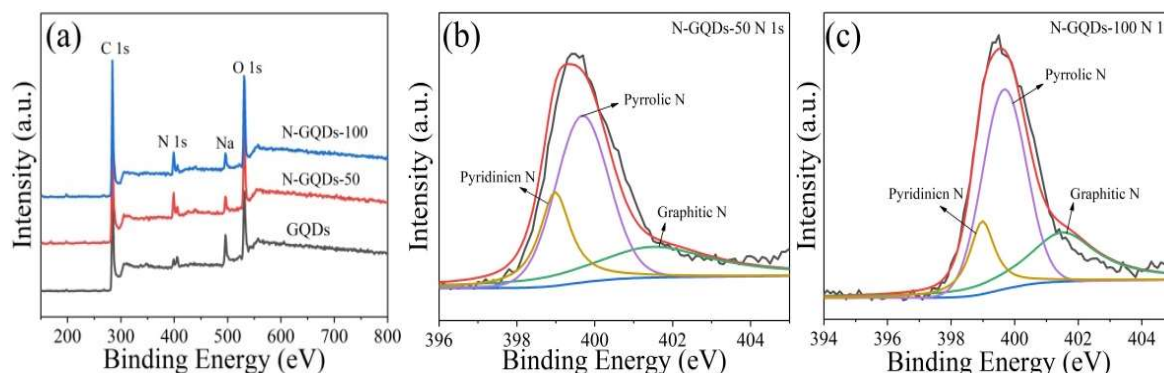


Figure 3. The full XPS spectra (a) of GQDs, N-GQDs-50 and N-GQDs-100. High-resolution N 1s spectrum of N-GQDs-50 (b) and N-GQDs-100 (c).

Table 1. The atomic percent (%) GQDs, N-GQDs-50 and N-GQDs-100 from XPS data.

Samples	C (at%)	O (at%)	N (at%)
GQDs	73.51	18.82	7.67
N-GQDs-50	71.41	17.95	10.64
N-GQDs-100	70.36	19.22	10.42

2.2. Optical Properties

Optical properties were used to characterize the physical nature of carbon-based materials. As shown in Figure 4, the optical absorption ability of GQDs (0.07 mg/mL) (Figure 4a) and N-GQDs-50 (0.07 mg/mL) (Figure 4b) was investigated by UV-vis spectrometer. GQDs displayed a wide absorption peak at 400–500 nm, which was similar to previous studies [44,45]. Compared to GQDs, N-GQDs-50 was also detected as having a strong absorption peak in the UV region at approximately 344 nm. Obviously, differences between GQDs and N-GQDs-50 in UV-vis spectra indicated that GQDs doped with N atom resulted in a strong absorption peak in the UV range.

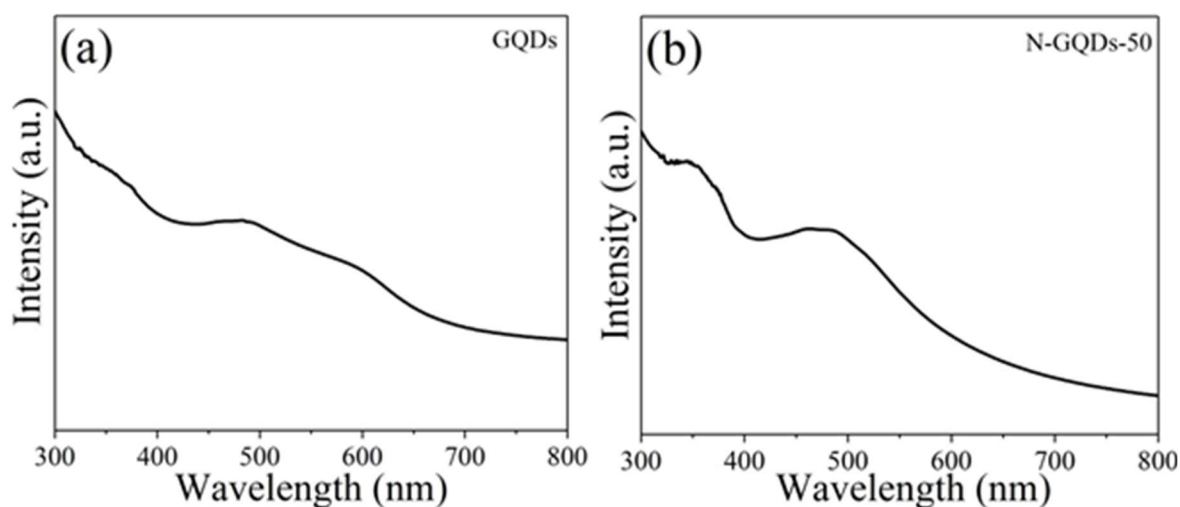


Figure 4. The UV-vis absorption spectra of the GQDs (a) and N-GQDs-50 (b).

According to the results of UV-vis absorption spectrum, the excitation wavelength of 310–390 nm was chosen for photoluminescent (PL) measurement. In this experiment, both GQDs and

N-GQDs-50 displayed excitation-independent PL behaviors, which were contrary to previous work on carbon-based fluorescent materials [41]. The emission peak of GQDs (Figure 5a) was approximately 540 nm and N-GQDs-50 (Figure 5b) was observed at approximately 520 nm. The excitation wavelength of 350 nm, with an emission peak of N-GQDs had blue shifted 20 nm compared to the GQDs in Figure 5c, which was most likely due to the reduction in size of N-GQDs-50 (see inserts of Figure 1a,b). This phenomenon is consistent with the trend observed by other quantum dots due to the quantum confinement effect at smaller particle size [46]. Figure 5d shows the PLE spectrum of N-GQDs-50 under the emission wavelength at 520 nm. One of the peaks was observed at 388 nm, which was in accordance with the PL results.

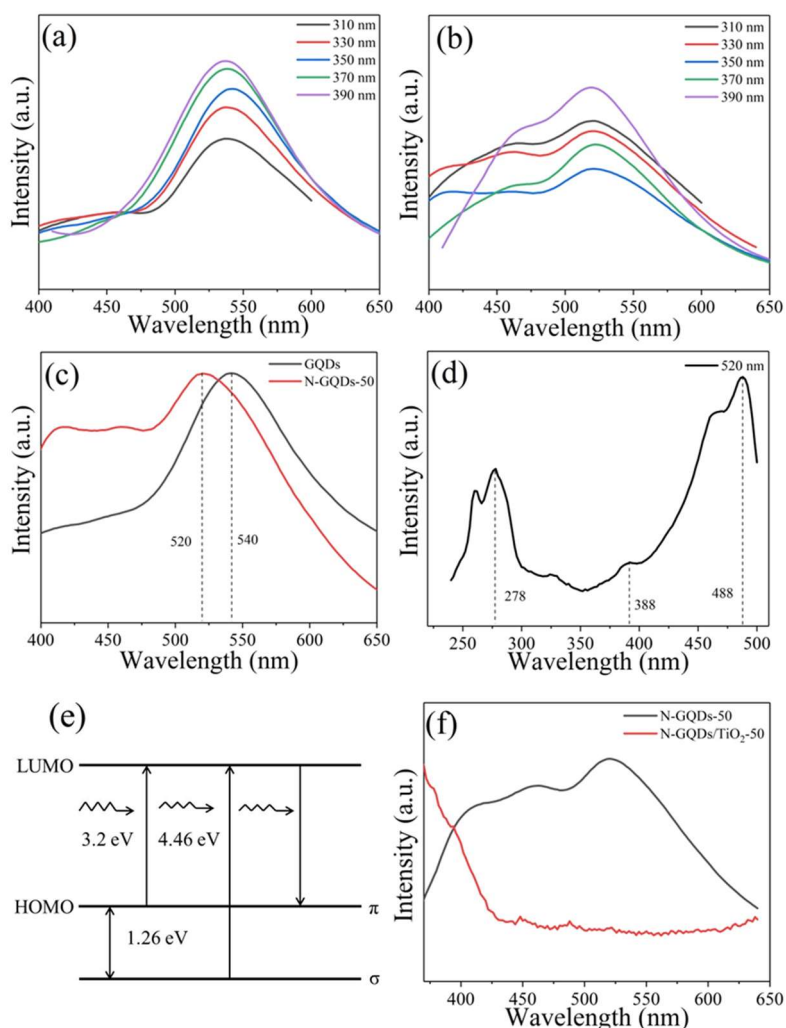


Figure 5. The PL spectra of GQDs (a) and N-GQDs-50 (b) under excitation with 310–390 nm. (c) Comparison of GQDs with N-GQDs under irradiation with 360 nm wavelength. (d) PLE spectra of N-QDs-50 when fixing emission wavelength at 520 nm. (e) Typical electronic transitions of triple carbenes in the optical spectrum of N-GQDs. (f) Comparison of N-GQDs-50 with N-GQDs/TiO₂-50 under irradiation with 330 nm wavelength.

The photoluminescence excitation (PLE) spectra showed that luminescence from N-GQDs could correspond to transitions at 278 (4.46 eV) and 388 (3.2 eV) nm, which could have been the result of transition between the σ and π orbital (HOMO) to the lowest unoccupied molecular orbital (LUMO), as shown in Figure 5e. Fluorescence performance was improved by the combination with photo-generated carriers. However, one way to improve photocatalytic performance was to inhibit the recombination of photo-generated carriers so that they could react with organic pollutants on

the surface of photocatalysts. Thus, Figure 5f shows that N-GQDs/TiO₂-50 possesses excellent photocatalytic activity. The multiplicity of carbene ground-state was connected with energy differences (δE) between the σ and π orbital. According to previous reports, δE should be less than 1.5 eV [47]. In our study, δE of N-GQDs was 1.26 eV, which demonstrated that δE was within the theoretical value.

2.3. Photocatalytic Activity and Possible Mechanism for Improving Photocatalytic Activity

The concentration C/C_0 of undegraded MO was used to indicate photocatalytic performance of different catalysts. MO without a catalyst degrades differently under UV light in Figure 6a,b. Pure TiO₂ nanoparticles displayed fine photocatalytic activity by UV irradiation, and the degradation rate of MO reached approximately 57% within 12 min. The photocatalytic performance of GQDs/TiO₂ was higher than pure TiO₂, which reached about 65%. Although the photocatalytic performance of GQDs/TiO₂ was preferable to that of pure TiO₂, the effect was not satisfactory. MO degradation by N-GQDs/TiO₂ was much higher than that of other catalysts. In particular, the degradation of MO by N-GQDs/TiO₂-50 reached 95% within 12 min, indicating that the content of graphitic N played a significant function on photocatalytic activity. As shown in Table 2, with the increase of ammonia water content, the content of pyrrolic N obviously increased, while the content of pyridinic N and graphitic N were lessened. The content of pyridinic N and graphitic N of N-GQDs-50 were higher than that of N-GQDs-100, up to 22.47% and 31.4%, respectively.

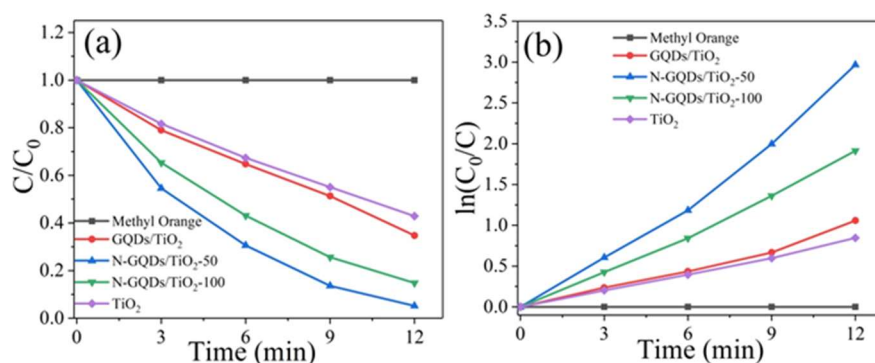


Figure 6. (a) The relationship between the concentration of undegraded MO and illumination time for different photocatalysts. (b) The relationship between the logarithm of C/C_0 and irradiation time of different photocatalysts.

Table 2. The content (%) of doped-N and the different N species of N-GQDs-50 and N-GQDs-100.

Samples	N (at%)	Pyridinic N (at%)	Pyrrolic N (at%)	Graphitic N (at%)
N-GQDs-50	10.64	22.47	44.09	31.44
N-GQDs-100	10.42	16.38	53.03	30.59

To further study the ability and stability of photocatalytic MO degradation by N-GQDs/TiO₂ composites, the cyclic stability experiment of photocatalytic degradation of MO by N-GQDs/TiO₂-50 was investigated (Figure 7a). After five cycles, the N-GQDs/TiO₂-50 was yet to show a good photocatalytic effect. As shown in Figure 7b, the photocatalytic performance of N-GQDs/TiO₂-50 and pure TiO₂ was slightly reduced, but the photocatalytic activity was still excellent, reaching over 90%. Their results show that the photocatalytic activity of TiO₂ could be greatly enhanced by modifying TiO₂ with effective methods.

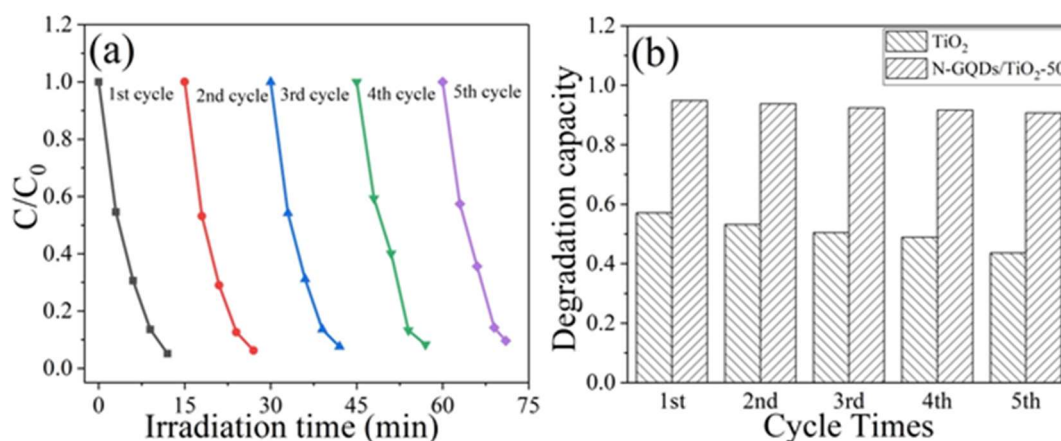
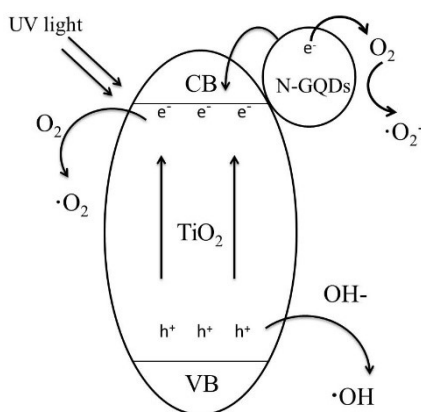


Figure 7. (a) Recycle stability of the photocatalytic decomposition of MO by N-GQDs/TiO₂-50. (b) Repetitive photocatalytic decomposition of MO for TiO₂ and N-GQDs/TiO₂-50 photocatalysts.

Scheme 1 explains the probable mechanism of degradation of MO by N-GQDs/TiO₂ composites. As an n-type semiconductor, TiO₂ was able to create electron-hole pairs [44]. Under UV irradiated light, the electron of TiO₂ transferred from the valence band to the conduction band to form an electro-hole. Electro-holes reacted with absorbed O₂/OH⁻ to produce $\cdot\text{O}_2$ / $\cdot\text{OH}$ so as to degrade MO. N-GQDs attached to the surface of TiO₂, absorbing UV light and raising the excitation of electrons. The excited electrons then transferred to the conduction band of TiO₂. With TiO₂ as the base of catalytic reaction, the N-GQDs as an unexceptionable electron migration area on the surface of TiO₂ could effectively and rapidly transmit photogenerated electrons, inhibiting the fast binding of photogenerated electron-hole pairs, and thus greatly improved the catalytic efficiency of TiO₂. Compared with GQDs, N-GQDs showed a strong absorption peak in the UV region. Therefore, N-GQDs/TiO₂ displayed strong photocatalytic activity by UV light. The oxygen in MO also combined with electrons on N-GQDs to generate $\cdot\text{O}_2^-$, which may have played a significant role in photocatalytic activity [6]. As the main N-binding configuration, pyridine N only existed at the edge of the GQDs, which could be used as the oxygen-reduction active site to enhance the activity of a catalyst. Furthermore, the graphitic N was the electron transfer site [43]. Thus, N-GQDs/TiO₂ displayed good photocatalytic performance, and the pyridinic N and graphitic N played a significant position in photocatalytic performance.



Scheme 1. The possible photocatalyst mechanism of N-GQDs/TiO₂ under UV light.

3. Experimental Section

3.1. Chemicals

All reagents were not processed further. Pyrene (C₆H₆), anhydrous alcohol (C₂H₅OH), sodium hydroxide (NaOH), nitric acid (HNO₃) ammonia water, titanium dioxide (TiO₂) were purchased

from reagent agent (manufacturer, city, country). Deionized water was used in all the experimental processes. All the chemicals were purchased from Shanghai, China.

3.2. Preparation of N-GQDs

GQDs were prepared using a simple hydrothermal method [48]. Then N-GQDs samples (N-GQDs-50, N-GQDs-100, -numbers represent the volume of the added ammonia water) were synthesized by a simple hydrothermal method. Briefly, 0.1 g GQDs was dispersed in 50 mL H₂O, and added to different volumes of ammonia water (50 mL and 100 mL). The mixed homogeneous solution was transferred into a Teflon-lined steel autoclave and then heated at 180 °C for 12 h. After cooling to room temperature, the obtained solution was filtered with a 0.22 µm filter membrane, and the filtered solution was dialyzed for 24 h using a 3500 Da dialysis bag to remove excess ions. Finally, the obtained N-GQDs were dried at 70 °C in air for the subsequent experiment.

3.3. Preparation of N-GQDs/TiO₂

N-GQDs/TiO₂ composites were synthesized by a simple hydrothermal method. Weighed 0.4 g Degussa P25 TiO₂ was dispersed into 200 mL N-GQDs aqueous solution (0.2 mg/mL) by ultrasonication (500 W, 40 kHz) for 30 min. Then the solution was transferred into Teflon-lined steel autoclave and then heated at 180 °C for 24 h. After cooling to room temperature, the product was washed three times by centrifugation with deionized water and anhydrous alcohol, then the collected sediment was dried at 70 °C in air to obtain the N-GQDs/TiO₂-50 composite. The GQDs/TiO₂ and N-GQDs/TiO₂-100 composites were also synthesized under the same conditions for comparison.

3.4. Photocatalytic Activity Measurements

The photocatalytic performance of the obtained samples was explored by degrading MO in quartz tubes at the UV light irradiation of a 600 W mercury lamp, and the photocatalytic experiment was carried out at room temperature. The distance between solution and lamp was 10 cm. The experimental procedure is as described: 50 mg samples were dissolved in 50 mL MO (5 mg/L). The resulting solution was roughened without treatment for an hour to achieve adsorption and desorption equilibrium between the catalyst and MO. Then the solution was put under the mercury lamp for illumination with magnetic stirring and 4 mL solution was removed every 3 min to a centrifuge for 5 min (8000 rpm) to remove catalyst particles. The concentration of MO after centrifugation was measured by a UV/vis/near infrared (NIR) spectrometer. The expression formula of degradation rate of MO is $\frac{C_0 - C}{C_0}$. The concentration of undegraded MO can be expressed as C/C_0 . In this study, C represents the concentration of MO after irradiation, C_0 represents the original concentration of MO before irradiation.

3.5. Characterization

Morphology of samples was measured by transmission electron microscopy (TEM, HT7700, Hitachi, Tokyo, Japan), and X-ray photoelectron spectroscopy (XPS) data were characterized by an ESCALAB 250Xi electron spectrometer (ThermoFisher Scientific, Waltham, MA, USA) with Al K α Radiation (1486.6 eV). X-ray diffraction (XRD) patterns of samples were recorded within 5–80° (2 θ) using a Rigaku D/MAX 2550 diffractometer (Rigaku, Tokyo, Japan) carried out at 40 kV and 100 mA. Fourier transform infrared spectroscopy (FT-IR) was investigated using a Perkin-Elmer spectrum. The UV-vis absorption spectrum was measured by using a UV/vis/NIR spectrometer (Perkin-Elmer, Lambda 750, PerkinElmer, Shelton, CT, USA). The photoluminescent (PL) and photoluminescence excitation (PLE) spectra (Carry Eclipse Fluorescence Spectrophotometer, Agilent Technologies Ltd., Cheshire, UK) were carried out using a fluorescence spectrophotometer.

4. Conclusion

In this study, we synthesized N-GQDs/TiO₂ composites by two facile hydrothermal methods. The results show that N-GQDs/TiO₂ exhibit excellent photocatalytic performance, and the ability to degrade MO for cyclic stability. In addition, the photocatalytic activity of N-GQDs/TiO₂ is associated with the content of graphitic N and the higher content, the better of photocatalytic activity. In particular, it was found that when the amount of ammonia water added was 50 mL and the contents of pyridinic N and graphitic N were as high as 22.47% and 31.44%, respectively. The photocatalytic performance of N-GQDs/TiO₂-50 reached about 95% in 12 min. This accomplishment may provide a new perspective for the future study of composites based on N-GQDs.

Author Contributions: Correspondence author, M.L. and L.W.; Data curation, F.L.; investigation, X.L. and J.Z.; methodology, F.L. and M.L. and Y.L.; supervision, M.L. (correspondence author) and L.W.; writing (original draft), F.L.; writing (review and editing), L.W.

Acknowledgments: This work was financially supported by the National Natural Science Foundation of China (Nos. 11764011, 21671129, 51472241, 21571124) and Natural Science Foundation of Guangxi Province (No. 2016GXNSFAA380008, 2017GXNSFBA198216), P. R. China.

Conflicts of Interest: The authors declare no competing financial interest.

References

1. Kumar, S.G.; Devi, L.G. Review on modified TiO₂ photocatalysis under UV/visible light: selected results and related mechanisms on interfacial charge carrier transfer dynamics. *J. Phys. Chem. Coruña* **2011**, *115*, 13211–13241. [[CrossRef](#)] [[PubMed](#)]
2. Cheng, H.; Fuku, K.; Kuwahara, Y.; Mori, K.; Yamashita, H. Harnessing single-active plasmonic nanostructures for enhanced photocatalysis under visible light. *J. Mater. Chem. Coruña* **2015**, *3*, 5244–5258. [[CrossRef](#)]
3. Luo, Y.; Li, M.; Hu, G.; Tang, T.; Wen, J.; Li, X.; Wang, L. Enhanced photocatalytic activity of sulfur-doped graphene quantum dots decorated with TiO₂ nanocomposites. *Mater. Res. Bull.* **2018**, *97*, 428–435. [[CrossRef](#)]
4. Bhatia, S.; Verma, N. Photocatalytic activity of ZnO nanoparticles with optimization of defects. *Mater. Res. Bull.* **2017**, *95*, 468–476. [[CrossRef](#)]
5. Wang, X.; Kafizas, A.; Li, X.; Moniz, S.J.A.; Reardon, P.J.T.; Tang, J.; Parkin, I.P.; Durrant, J.R. Transient absorption spectroscopy of anatase and rutile: The impact of morphology and phase on photocatalytic activity. *J. Phys. Chem. C* **2015**, *119*, 10439–10447. [[CrossRef](#)]
6. Konstantinou, I.K.; Albanis, T.A. TiO₂-assisted photocatalytic degradation of azo dyes in aqueous solution: kinetic and mechanistic investigations: A review. *Appl. Catal. B Environ.* **2004**, *49*, 1–14. [[CrossRef](#)]
7. Ruggieri, F.; Antonio D'Archivio, A.; Fanelli, M.; Santucci, S. Photocatalytic degradation of linuron in aqueous suspensions of TiO₂. *RSC Adv.* **2011**, *1*, 611–618. [[CrossRef](#)]
8. Wei, H.; Wang, L.; Li, Z.; Ni, S.; Zhao, Q. Synthesis and photocatalytic activity of one-dimensional CdS@TiO₂ core-shell heterostructures. *Nano-Micro Lett.* **2011**, *3*, 6–11. [[CrossRef](#)]
9. Ruggieri, F.; Di Camillo, D. Electrospun Cu-, W- and Fe-doped TiO₂ nanofibres for photocatalytic degradation of rhodamine 6G. *J. Nanopart. Res.* **2013**, *15*, 1982. [[CrossRef](#)]
10. Sawunyama, P.; Yasumori, A.; Okada, K. The nature of multilayered TiO₂-based photocatalytic films prepared by a sol-gel process. *Mater. Res. Bull.* **1998**, *33*, 795–801. [[CrossRef](#)]
11. Mori, R.; Takahashi, M.; Yoko, T. 2D spinodal phase-separated TiO₂ films prepared by sol-gel process and photocatalytic activity. *Mater. Res. Bull.* **2004**, *39*, 2137–2143. [[CrossRef](#)]
12. Asahi, R.; Morikawa, T.; Ohwaki, T.; Aoki, K.; Taga, T. Visible-light photocatalysis in nitrogen-doped titanium oxides. *Science* **2001**, *293*, 269–271. [[CrossRef](#)] [[PubMed](#)]
13. Mori, K.; Kawashima, M.; Yamashita, H. Visible-light-enhanced Suzuki-miyaura coupling reaction by cooperative photocatalysis with an Ru-Pd bimetallic complex. *Chem. Commun.* **2014**, *50*, 14501–14503. [[CrossRef](#)] [[PubMed](#)]
14. Yuan, Y.-P.; Yin, L.-S.; Cao, S.-W.; Xu, G.-S.; Li, C.-H.; Xue, C. Improving photocatalytic hydrogen production of metal-organic framework UiO-66 octahedrons by dye-sensitization. *Appl. Catal. B Environ.* **2015**, *168–169*, 572–576. [[CrossRef](#)]

15. Wang, P.; Wang, J.; Ming, T.; Wang, X.; Yu, H.; Yu, J.; Wang, Y.; Lei, M. Dye-sensitization-induced visible-light reduction of graphene oxide for the enhanced TiO₂ photocatalytic performance. *ACS Appl. Mater. Interfaces* **2013**, *5*, 2924–2929. [[CrossRef](#)] [[PubMed](#)]
16. Sadhu, S.; Poddar, P. Template-free fabrication of highly-oriented single-crystalline 1D-rutile TiO₂- MWCNT composite for enhanced photoelectrochemical activity. *J. Phys. Chem. C* **2014**, *118*, 19363–19373. [[CrossRef](#)]
17. Wan, L.; Long, M.; Zhou, D.; Zhang, L.; Cai, W. Preparation and characterization of freestanding hierarchical porous TiO₂ monolith modified with graphene oxide. *Nano-Micro Lett.* **2012**, *4*, 90–97. [[CrossRef](#)]
18. Yu, H.; Liu, R.; Wang, X.; Wang, P.; Yu, J. Enhanced visible-light photocatalytic activity of Bi₂WO₆ nanoparticles by Ag₂O cocatalyst. *Appl. Catal. B Environ.* **2012**, *111–112*, 326–333. [[CrossRef](#)]
19. Wang, P.; Xia, Y.; Wu, P.; Wang, X.; Yu, H.; Yu, J. Cu(II) as a general cocatalyst for improved visible-light photocatalytic performance of photosensitive ag-based compounds. *J. Phys. Chem. C* **2014**, *118*, 8891–8898. [[CrossRef](#)]
20. Gu, Y.; Xing, M.; Zhang, J. Synthesis and photocatalytic activity of graphene based doped TiO₂ nanocomposites. *Appl. Surf. Sci.* **2014**, *319*, 8–15. [[CrossRef](#)]
21. Aleksandrak, M.; Adamski, P.; Kukułka, W.; Zielinska, B.; Mijowska, E. Effect of graphene thickness on photocatalytic activity of TiO₂-graphene nanocomposites. *Appl. Surf. Sci.* **2015**, *331*, 193–199. [[CrossRef](#)]
22. Seh, Z.W.; Liu, S.; Low, M.; Zhang, S.-Y.; Liu, Z.; Mlayah, A.; Han, M.-Y. Janus Au-TiO₂ Photocatalysts with Strong Localization of Plasmonic Near-Fields for Efficient Visible-Light Hydrogen Generation. *Adv. Mater.* **2012**, *24*, 2310–2314. [[CrossRef](#)] [[PubMed](#)]
23. Zheng, Z.; Huang, B.; Qin, X.; Zhang, X.; Dai, Y.; Whangbo, M.-H. Facile in situ synthesis of visible-light plasmonic photocatalysts M@TiO₂ (M = Au, Pt, Ag) and evaluation of their photocatalytic oxidation of benzene to phenol. *J. Mater. Chem.* **2011**, *21*, 9079–9087. [[CrossRef](#)]
24. Wang, L.; Wu, B.; Li, W.; Wang, S.; Li, Z.; Li, M.; Pan, D.; Wu, M. Amphiphilic graphene quantum dots as self-targeted fluorescence probes for cell nucleus imaging. *Adv. Biosyst.* **2018**, *2*, 1700191. [[CrossRef](#)]
25. Pan, D.; Jiao, J.; Li, Z.; Guo, Y.; Feng, C.; Liu, Y.; Wang, L.; Wu, M. Efficient separation of electron-hole pairs in graphene quantum dots by TiO₂ heterojunctions for dye degradation. *ACS Sustain. Chem. Eng.* **2015**, *3*, 2405–2413.
26. Fei, H.; Ye, R.; Ye, G.; Gong, Y.; Peng, Z.; Fan, X.; Samuel, E.L.G.; Ajayan, P.M.; Tour, J.M. Boron- and nitrogen-doped graphene quantum dots/graphene hybrid nanoplatelets as efficient electrocatalysts for oxygen reduction. *ACS Nano* **2014**, *8*, 10837–10843. [[CrossRef](#)] [[PubMed](#)]
27. Tang, L.; Wang, J.; Jia, C.; Lv, G.; Xu, G.; Li, W.; Wang, L.; Zhang, J.; Wu, M. Simulated solar driven catalytic degradation of psychiatric drug carbamazepine with binary BiVO₄ heterostructures sensitized by graphene quantum dots. *Appl. Catal. B Environ.* **2017**, *205*, 587–596. [[CrossRef](#)]
28. Yeh, T.-F.; Teng, C.-Y.; Chen, S.-J.; Teng, H. Nitrogen-doped graphene oxide quantum dots as photocatalysts for overall water-splitting under visible light illumination. *Adv. Mater.* **2014**, *26*, 3297–3303. [[CrossRef](#)] [[PubMed](#)]
29. Li, F.; Sun, L.; Luo, Y.; Li, M.; Xu, Y.; Hu, G.; Li, X.; Wang, L. Effect of thiophene S on the enhanced ORR electrocatalytic performance of sulfur-doped graphene quantum dot/reduced graphene oxide nanocomposites. *RSC Adv.* **2018**, *8*, 19635–19641. [[CrossRef](#)]
30. Sun, L.; Luo, Y.; Li, M.; Hu, G.; Xu, Y.; Tang, T.; Weng, J.; Li, X.; Wang, L. Role of pyridinic-N for nitrogen-doped graphene quantum dots in oxygen reaction reduction. *J. Colloid Interface Sci.* **2017**, *508*, 154–158. [[CrossRef](#)] [[PubMed](#)]
31. Dong, J.; Wang, K.; Sun, L.; Sun, B.; Yang, M.; Chen, H.; Wang, Y.; Sun, J.; Dong, L. Application of graphene quantum dots for simultaneous fluorescence imaging and tumor-targeted drug delivery. *Sens. Actuators B Chem.* **2018**, *256*, 616–623. [[CrossRef](#)]
32. Wang, L.; Li, W.; Wu, B.; Li, Z.; Pan, D.; Wu, M. Room-temperature synthesis of graphene quantum dots via electron-beam irradiation and their application in cell imaging. *Chem. Eng. J.* **2017**, *309*, 374–380. [[CrossRef](#)]
33. Wang, L.; Wu, B.; Li, W.; Li, Z.; Zhan, J.; Geng, B.; Wang, S.; Pan, D.; Wu, M. Industrial production of ultra-stable sulfonated graphene quantum dots for Golgi apparatus imaging. *J. Mater. Chem. B* **2017**, *5*, 5355–5361. [[CrossRef](#)]
34. Wang, L.; Li, W.; Li, M.; Su, Q.; Li, Z.; Pan, D.; Wu, M. Ultrastable amine, sulfo cofunctionalized graphene quantum dots with high two-photon fluorescence for cellular imaging. *ACS Sustain. Chem. Eng.* **2018**, *6*, 4711–4716. [[CrossRef](#)]

35. Li, W.; Li, M.; Liu, Y.; Pan, D.; Li, Z.; Wang, L.; Wu, M. Three-minute ultrarapid microwave-assisted synthesis of bright fluorescent graphene quantum dots for live cell staining and white LEDs. *ACS Appl. Nano Mater.* **2018**, *1*, 1623–1630. [[CrossRef](#)]
36. Li, L.; Yan, X. Colloidal graphene quantum dots. *J. Phys. Chem. Lett.* **2010**, *1*, 2572–2576. [[CrossRef](#)]
37. Rajender, G.; Kumar, J.; Giri, P.K. Interfacial charge transfer in oxygen deficient TiO₂-graphene quantum dot hybrid and its influence on the enhanced visible light photocatalysis. *Appl. Catal. B Environ.* **2018**, *224*, 960–972. [[CrossRef](#)]
38. Safardoust-Hojaghan, H.; Salavati-Niasari, M. Degradation of methylene blue as a pollutant with N-doped graphene quantum dot/titanium dioxide nanocomposite. *J. Clean. Prod.* **2017**, *148*, 31–36. [[CrossRef](#)]
39. Tian, H.; Shen, K.; Hu, X.; Qiao, L.; Zheng, W. N, S co-doped graphene quantum dots-graphene-TiO₂ nanotubes composite with enhanced photocatalytic activity. *J. Alloys Compd.* **2017**, *691*, 369–377. [[CrossRef](#)]
40. Zhang, B.-X.; Gao, H.; Li, X.-L. Synthesis and optical properties of nitrogen and sulfur co-doped graphene quantum dots. *New J. Chem.* **2014**, *38*, 4615–4621. [[CrossRef](#)]
41. Wang, Y.; Zhang, L.; Liang, R.-P.; Bai, J.-M.; Qiu, J.-D. Using graphene quantum dots as photoluminescent probes for protein kinase sensing. *Anal. Chem.* **2013**, *85*, 9148–9155. [[CrossRef](#)] [[PubMed](#)]
42. Taibi, M.; Ammar, S.; Jouini, N.; Fiévet, F.; Molinié, P.; Drillon, M. Layered nickel hydroxide salts: Synthesis, characterization and magnetic behaviour in relation to the basal spacing. *J. Mater. Chem.* **2002**, *12*, 3238–3244. [[CrossRef](#)]
43. Xu, Y.; Mo, Y.; Tian, J.; Wang, P.; Yu, H.; Yu, J. The synergistic effect of graphitic N and pyrrolic N for the enhance photocatalytic performance of nitrogen-doped graphene/TiO₂ nanocomposites. *Appl. Catal. B Environ.* **2016**, *181*, 810–817. [[CrossRef](#)]
44. Dong, Y.; Chen, C.; Zheng, X.; Gao, L.; Cui, Z.; Yang, H.; Guo, C.; Chi, Y.; Li, C.M. One-step and high yield simultaneous preparation of single- and multi-layer graphene quantum dots from CX-72 carbon black. *J. Mater. Chem.* **2012**, *22*, 8764–8766. [[CrossRef](#)]
45. Ye, R.; Xiang, C.; Lin, J.; Peng, Z.; Huang, K.; Yan, Z.; Cook, N.P.; Samuel, E.L.G.; Hwang, C.-C.; Ruan, G.; et al. Coal as an abundant source of graphene quantum dots. *Nat. Commun.* **2013**, *4*, 2943. [[CrossRef](#)] [[PubMed](#)]
46. Melnikov, D.V.; Chelikowsky, J.R. Quantum confinement in phosphorus-doped silicon nanocrystals. *Phys. Rev. Lett.* **2004**, *92*, 046802. [[CrossRef](#)] [[PubMed](#)]
47. Peng, J.; Gao, W.; Gupta, B.K.; Liu, Z.; Aburto, R.-R.; Ge, L.; Song, L.; Alemany, L.B.; Zhan, X.; Gao, G.; et al. Graphene quantum dots derived from carbon fibers. *Nano Lett.* **2012**, *12*, 844–849. [[CrossRef](#)] [[PubMed](#)]
48. Wang, L.; Wang, Y.; Xu, T.; Liao, H.; Yao, C.; Liu, Y.; Li, Z.; Chen, Z.; Pan, D.; Sun, L.; Wu, M. Gram-scale synthesis of single-crystalline graphene quantum dots with superior optical properties. *Nat. Commun.* **2014**, *5*, 5357. [[CrossRef](#)] [[PubMed](#)]

